Isotactic Polypropylene Morphology–Raman Spectra Correlations

XUEQIN WANG, STEPHEN MICHIELSEN

Polymer Education and Research Center, School of Textile & Fiber Engineering, Georgia Institute of Technology, Atlanta, Georgia 30332-0295

Received 31 July 2000; accepted 4 December 2000

ABSTRACT: Isotactic polypropylene (iPP) is used in a wide variety of products, including the rapidly growing area of nonwoven fabrics. A new method based on Raman microspectroscopy is developed to determine the morphology of iPP fibers in complex structures through correlations with specific features of the Raman spectra and the birefringence and Lorentz density of a series of fibers. A good correlation is found between the fourth Legendre polynomial (P_4) of the principle axis of the Raman tensor of the 841 cm^{-1} band and the birefringence. Only vibrations that include the C—C—C backbone stretch correlate well with the birefringence. There is a second, empirical correlation between the birefringence and the depolarization ratios of the 841 and 809 cm^{-1} Raman bands when the fiber axis is oriented parallel to the laser polarization. The experimental protocol for this empirical correlation is much simpler than for the P_4 correlation while simultaneously yielding improved accuracy. There is another empirical correlation between the Lorentz density and the depolarization ratios of the 841 and 1330 cm^{-1} Raman bands. Thus, the birefringence and Lorentz density of iPP fibers could be determined quantitatively using polarized Raman microspectroscopy. © 2001 John Wiley & Sons, Inc. J Appl Polym Sci 82: 1330–1338, 2001

Key words: isotactic polypropylene; Raman microspectroscopy; orientation; birefringence; density; depolarization; second Legendre polynomial; fourth Legendre polynomial

INTRODUCTION

The crystallinity and the extent of orientation of molecular chains are two of the most important morphological characteristics of the fiber structure that influence the final properties. The orientation of polymer chains in a fiber is frequently estimated using birefringence. Crystallinity can be estimated by a number of different techniques such as X-ray diffraction, calorimetric analysis, and density measurements. Each method provides a different measure of crystallinity and generally cannot be directly compared. None of these methods has been shown to be more accurate than the others. However, they usually give the same trends in the crystallinity. In complex structures such as nonwoven fabrics, these methods are difficult to perform with the desired precision.

The X-ray scattering of fibers requires a large number of parallel fibers to obtain the high quality diffraction patterns needed for morphology characterization. Birefringence requires individual fibers of a few centimeters length. Differential scanning calorimetry requires approximately 10 mg of fibers. Because of the difficulty of extracting fibers from a nonwoven fabric, none of these methods are suitable for determining the mor-

Correspondence to: S. Michielsen.

Contract grant sponsor: Nonwoven Cooperative Research Center.

Journal of Applied Polymer Science, Vol. 82, 1330–1338 (2001)

phology of these fibers. Moreover, with the development of specialty fibers such as bicomponent fibers, fibers having noncircular cross sections, melt-blown fibers, and crimped fibers, it has become difficult or impossible to use conventional techniques for crystallinity and orientation measurements.[1] A new, reliable method for measuring the morphology within complex structures is needed.

One potential method is Raman microspectroscopy. Improvements in instrumentation have resulted in many new instruments capable of measuring the Raman spectrum on extremely small samples.[2,3] Raman microspectroscopy requires virtually no sample preparation and has a spatial resolution of <5 μm. It has been used to study the morphology of several polymers, such as poly(ethylene terephthalate)[2] and nylon.[4] Raman spectroscopy can also provide the second and fourth Legendre polynomials (P_2 and P_4) of the molecular vibration associated with the Raman band under study.[5] The average values of P_2 and P_4 for Raman scattering are defined as

$$\langle P_2 \rangle = \frac{\langle 3\ \cos^2\theta - 1 \rangle}{2}$$

$$\langle P_4 \rangle = \frac{\langle 35\ \cos^4\theta - 30\ \cos^2\theta + 3 \rangle}{8} \qquad (1)$$

where the angle brackets indicate the average over all chains in the sampling volume and θ is the angle that the major axis of the Raman tensor for the vibration under consideration makes with the fiber axis. The birefringence is a function of P_2 of the polarizability and is given by[6]

$$\Delta n = \Delta n_p \langle P_2 \rangle_{\text{bir}} \qquad (2)$$

where Δn_p is the birefringence of perfectly oriented chains, $\langle P_2 \rangle_{\text{bir}}$ is identical in form to eq. (1), but the angle θ is now the angle between the fiber axis and the major axis of the polarizability tensor for the polymer chain. Because the molecular polarizability and the Raman tensor are both attached to the polymer chain, it should be possible to determine the birefringence via a correlation with the measured polarized Raman spectra.

One of the earliest uses of Raman spectroscopy on isotactic polypropylene (iPP) is the work of Hendra and Willis[7]; they attempted to determine the orientation of polymer chains within fibers and films. They showed that the Raman bands had different intensities when the fiber or stretch direction of the film was parallel to the excitation beam or perpendicular to it. Vasko and Koenig[8] determined the depolarization ratios for all of the vibrations of the monoclinic and semitic crystalline forms, as well as the melt. Satija and Wang[9] and Wang and Cavanaugh[10] used the depolarization ratios of the melt combined with the intensity ratios of oriented iPP rods to determine the average values of P_2 for the 841 and 1256 cm^{-1} bands and P_4 for the 1256 cm^{-1} band. They argued that the depolarization ratio of the unoriented material should be approximately the same in the melt and in the semicrystalline rod. They found that the P_2 of the 1256 cm^{-1} band was in good agreement with the birefringence of the extruded rod. De Baez et al.[11] found that the intensity of the band at 809 cm^{-1} increased relative to that at 842 cm^{-1} as the crystallinity increased, but both bands were also sensitive to the extent of chain orientation. Fraser and colleagues[12] also found that the bands at 809 and 842 cm^{-1} were broad in the samples of low crystallinity. The bands at 1152 and 1169 cm^{-1} were also sensitive to crystallinity. However, to date, no quantitative correlation of Raman spectra and iPP morphology exists. Presented below are new correlations between features of the polarized Raman spectra of iPP fibers and the birefringence and densities of these iPP fibers. These correlations enable quantitative measurements of the morphology on a much smaller size scale (~ 5 μm) than current methods. This permits the analysis of the morphology of core–shell or side by side bicomponent fibers in which at least one of the components is iPP, iPP nonwoven fabrics, or other complex structures containing iPP.

EXPERIMENTAL

Materials

Low denier iPP fibers were kindly provided by FiberVisions. The fiber samples were chosen to have a wide range of crystallinity and orientation to facilitate the development of robust morphology correlations. These original samples had a strong correlation between the density and the birefringence (Fig. 1). To reduce this effect, additional samples were made by annealing several of these yarns. A loop of an original iPP yarn was made. This loop was tied to a polyaramid yarn that was fastened to a fixed plate. The other end

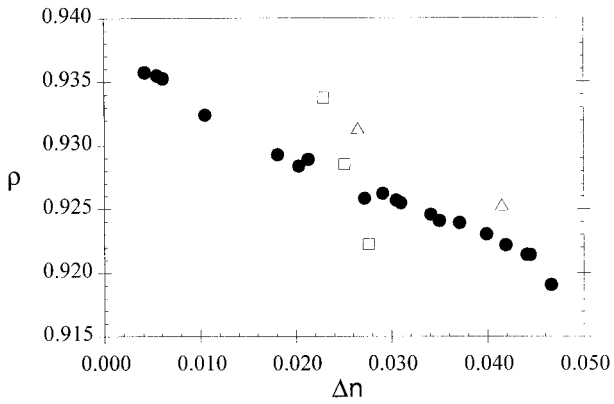

Figure 1 The correlation between the Lorentz density and the birefringence for the fibers used in this study: (●) original samples as provided by FiberVisions, Inc., (□) samples that were cold drawn, and (△) samples that were annealed (see text).

of the iPP loop was tied to another polyaramid yarn. This yarn was placed on a pulley and a 10-g weight was hung from it. A tubular heater was placed over the first polyaramid yarn and heated to 140°C. After equilibration, the heater was rolled into position over the iPP yarn for 3 min and then rolled back to its initial position. The process is shown in Figure 2. Subsequently, single fibers were removed from the yarn for analysis. Additional samples were made by cold drawing

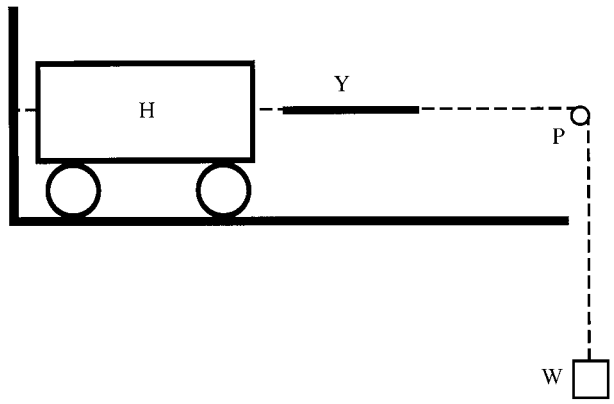

Figure 2 The annealing apparatus. The yarn (Y) that is to be annealed is attached to two polyaramid fibers. One polyaramid yarn is attached to a wall, and the other is passed over a low friction pulley (P) and a 10-g weight (W) is hung from it. The heater (H) is raised to the annealing temperature while placed over the polyaramid yarn on the left. After equilibrating, it is rolled to the right until the yarn to be annealed is in the center of the heater. After the desired annealing time, the heater is rolled back to the left.

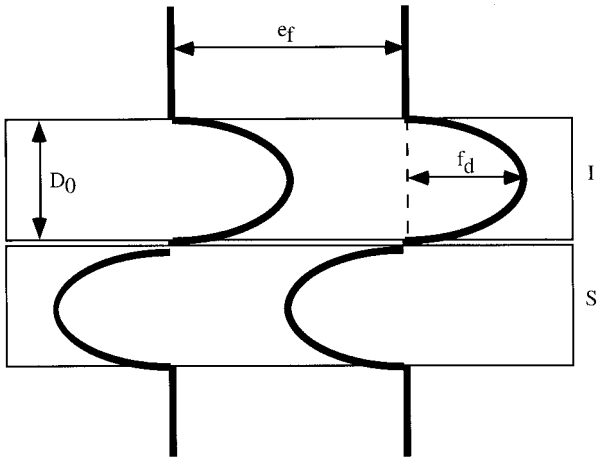

Figure 3 The interference fringes (heavy curves) are shown on the fiber image (I) and the sheared image (S); f_d, the fringe shift within the fiber; e_f, the equivalence factor; D_0, the initial fiber diameter. The f_d is for the polarization parallel to the fiber axis (i.e., $f_{d,\parallel}$).

some of the original yarns at 21°C and approximately 300 mm/min.

Measurements

Birefringence and Lorentz Density Measurement

The refractive indices parallel and perpendicular to the fiber axis were measured on an Aus Jena Interphako interference microscope. Ten filaments of an iPP sample were mounted on a glass slide and immersed in a refractive index oil (R. P. Cargille Laboratories, Inc.) having a refractive index between the parallel and perpendicular refractive indices of the sample (1.48–1.50). A coverslip was placed on top of the liquid. The filament was focused and aligned parallel to the left–right axis of the microscope. The image was then sheared until the two images were slightly separated. The slit apparatus was rotated until interference fringes could be seen. The fringes were aligned top to bottom in the eyepiece and adjusted so that the spacing between them was 15 eyepiece divisions. The 546-nm spectral line of a low pressure mercury lamp was selected with an interference filter. When light was polarized parallel to the sample, the refractive index of the sample was higher than that of the mounting liquid and the fringes were deflected to the right. Likewise, when light was polarized perpendicular to the sample, the fringes were deflected to the left. This is shown schematically in Figure 3. The refractive index of the sample in the parallel and perpendicular directions was calculated using[13]

$$n_{\parallel} = n_{\text{liq}} + \frac{f_{d,\parallel} \cdot e_f}{D_0}$$

$$n_{\perp} = n_{\text{liq}} - \frac{f_{d,\perp} \cdot e_f}{D_0} \quad (3)$$

where $n_{\parallel}$ and $n_{\perp}$ are the respective refractive indexes of the sample parallel and perpendicular to the fiber axis, n_{liq} is the refractive index of the mounting index liquid, e_f is the equivalence factor given by the ratio of the wavelength of light to the fringe spacing (in eyepiece divisions), and D_0 (nm) is the diameter of the fiber given by the product of the diameter in eyepiece divisions and the magnification. The birefringence (n) of the sample is the difference between $n_{\parallel}$ and $n_{\perp}$, which is calculated by

$$\Delta n = n_{\parallel} - n_{\perp} \quad (4)$$

Finally the Lorentz density of iPP (g/mL) was determined using the correlation developed by DeVries[14]:

$$\rho = 3.1827\left(\frac{n_{\text{iso}}^2 - 1}{n_{\text{iso}}^2 + 2}\right) \quad (5)$$

where n_{iso} is the isomorphic refractive index given by

$$n_{\text{iso}} = \frac{n_{\parallel} + 2n_{\perp}}{3} \quad (6)$$

The density is a quantitative measure of the crystallinity.

Polarized Laser Raman Microspectroscopy

Raman spectra were collected in the backscattering mode using a HoloLab Series 5000 Raman microscope coupled to a HoloLab Series 5000 Research Raman Spectrometer 785 using a 785-nm solid-state laser. The microscope objective performed the dual function of focusing the laser beam onto the sample and collecting and collimating the backscattered light. A holographic beam splitter was used to separate the Raman backscatter from the counterpropagating laser light. The backscatter was then further filtered with a holographic superNotch filter to block Rayleigh scattered light and was then focused through a 15-μm pinhole into an optical fiber with a core diameter of 100 μm and finally into the imaging spectrograph. The image of the fiber was displayed on a computer screen so that the sample could be viewed during sample alignment. All of the iPP Raman spectra were recorded using Kaiser Optical Systems HoloGRAMS software with a single exposure for 200 s with the cosmic ray filter on and dark noise subtraction on.

Single filaments were mounted on steel washers. To mount them flat, one end of the sample was glued to the washer. Slight tension was applied to the other end of the fiber, and it was then glued to the other side of the washer while still under tension. (Glass slides could not be used because of the strong phonon band from glass.) The washer was placed on a rotation mount to orient the fiber as desired. Raman spectra were recorded primarily with the use of a single mode collection fiber and a 50× objective. The fiber was aligned along the x or the y axis of the microscope by viewing the fiber image on the computer screen while rotating the fiber to the desired orientation.

Raman spectra were collected using a backscatter arrangement in all four of the geometries shown in Figure 4. Hence, the propagation directions of the incident and scattered laser beams were along the same axis. The input laser beam was polarized along the y axis and the fiber axis was oriented either along the y axis or along the x axis. The scattered light was passed through an analyzer polarizer, which could be oriented parallel to the incident light polarization or perpendicular to it. When the fiber was aligned along the y axis and the analyzer was parallel to the incident polarization, the $Y_{\parallel}$ spectrum was obtained. When the analyzer was perpendicular to the incident polarization, the $Y_{\perp}$ spectrum was obtained. Likewise, when the fiber was aligned along the x axis, the $X_{\parallel}$ and $X_{\perp}$ spectra were obtained. The polarization direction of the analyzer was changed by rotating the analyzer. Because the $Y_{\perp}$ and $X_{\perp}$ spectra should be identical for a cylindrically symmetric fiber,[15] they were used to normalize the intensities of the $Y_{\parallel}$ and $X_{\parallel}$ spectra. The different sensitivities for the two different polarizations ($\parallel$ and $\perp$) of the instrument were measured using the depolarization ratio of CCl_4. The perpendicular intensities were corrected by multiplying them by 0.628 because the instrument was more sensitive to this polarization.

Although the phase boundaries between crystalline and noncrystalline regions can lead to depolarization of the incident light due to scattering from the interfaces, we found that this effect was

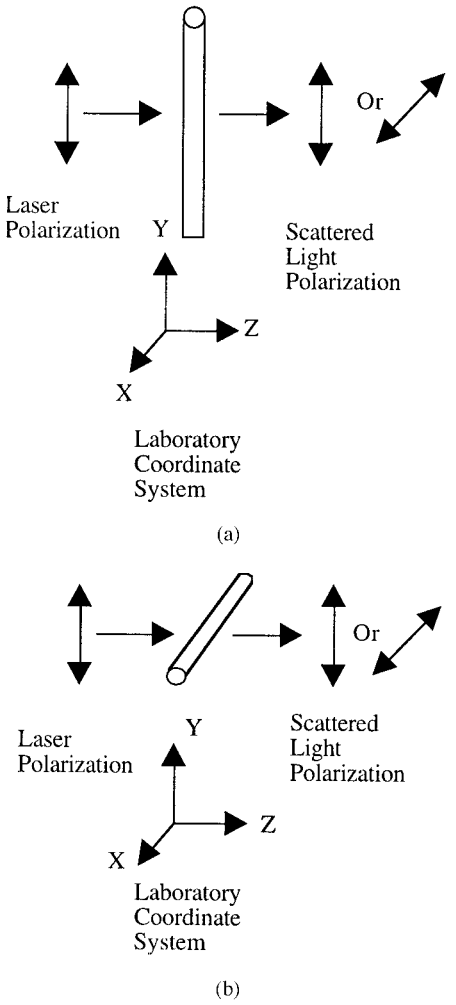

Figure 4 The scattering geometry is defined in laboratory coordinates where the incident laser propagates in the z direction with polarization in the y direction. The fiber axis may be aligned along the y axis or the x axis. The scattered light propagates in the negative z direction. An analyzing polarizer can be oriented to select only light polarized in the y direction or only in the x direction (i.e., polarized either parallel or perpendicular to the incident light polarization). The configurations for (a) $Y_{\parallel}$ and $Y_{\perp}$ and (b) $X_{\parallel}$ and $X_{\perp}$ are shown.

negligible in the samples we examined. We found the depolarization ratio of the 398 cm^{-1} band to be 0.087 for a high crystallinity, low birefringence sample, which was in good agreement with the values of 0.10 for the monoclinic crystalline form and 0.08 for the melt reported by Vasko and Koenig.[8]

An effort was made to collect data at the same point when the fiber axis was aligned in the X and Y orientations. Some unusual point in the fiber was set as zero, and a known distance was traversed along the fiber before collecting data. When the sample was rotated, the singular point in the fiber was again set as zero and an equal distance was traversed along the fiber, thus collecting data very near to, if not exactly at, the initial point. Figure 5 shows typical Raman spectra for a highly oriented fiber and one with a low degree of orientation.

Data Analysis

All Raman spectra were analyzed using the GRAMS/5 (Galactic Industries, Inc.) software package. The Raman bands at 399, 454, 809, 841, 974, 1152, 1169, 1330, 1438, and 1452 cm^{-1} of a Raman spectrum were fit using the curve-fit routine in GRAMS. This routine fit the peaks and gave the peak area, height, full width at half-maximum, position, and Gaussian and Lorentzian content for each peak. Each peak was fit multiple times with different initial conditions to ensure repeatability of the fit, and the peak areas were used for intensity. Raman spectra for all three specimens of each sample in each of the four configurations were used. Figure 6 shows a typical curve fit for the 1152 and 1169 cm^{-1} Raman bands of iPP.

The JMP (SAS Institute, Inc.) software package was used to perform multiple linear regression analysis to develop statistical models relating the birefringence and Lorentz density of the fibers to the various peak intensity ratios of their Raman spectra. The Raman data of all three fibers in each sample were incorporated into this analysis. The results obtained by the regression analysis were then verified by collecting the Raman spectrum of a new set of fibers, which con-

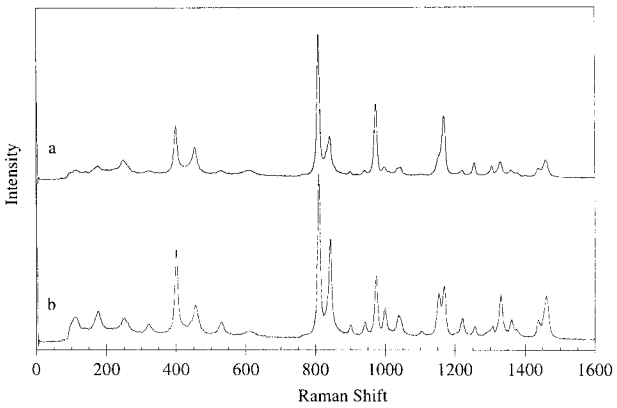

Figure 5 The iPP Raman spectra of high (spectrum a) and low (spectrum b) orientation fibers.

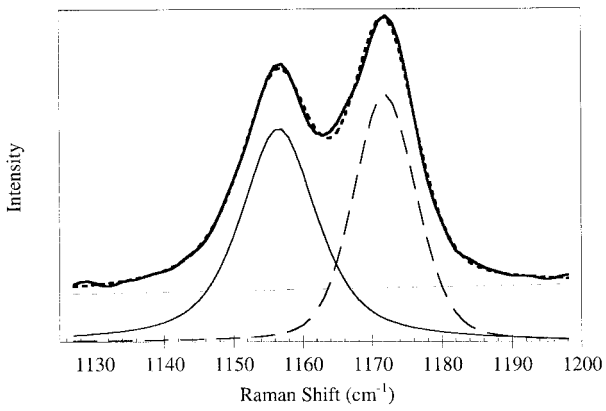

Figure 6 The curve fit for the 1120–1190 cm^{-1} region: (—) the original Raman curve; (- - -) the best curve fit for this region; (—) individual peak area for the 1152 cm^{-1} band; (– – –) individual peak area for the 1169 cm^{-1} band; and (- · -) the baseline.

sisted of iPP fibers prepared by varying only the spinning speeds. Again three specimens were used from each sample. The relations obtained for the birefringence and Lorentz density were employed to predict the properties of these fibers. The results were then compared to the values obtained from interference microscopy, and they agreed within experimental error.

RESULTS

The $Y_\parallel$ Raman spectra of two different fibers (high and low orientation fibers) are shown in Figure 5. It is obvious that there are many differences between these two spectra. These differences are used below to develop Raman spectra–morphology correlations. As noted previously, the birefringence is related to the P_2 of the polarizability of the chain segments within the fiber. The P_2 and P_4 of the Raman bands are related to the change in the polarizability for the individual molecular vibrations. Therefore, we postulate that the birefringence can be predicted quantitatively by the average values of P_2 and/or P_4 of one or more Raman bands.

The P_2 and P_4 can be determined from the measured Raman intensities after correcting for the instrumental polarization ratio as described in the Experimental section:

$$\langle P_2\rangle = \left\langle \frac{\left[-36\left(\frac{\alpha}{\beta}\right)^2 - 8\right]\frac{I_{X_\parallel}}{I_{X_\perp}} + \left[36\left(\frac{\alpha}{\beta}\right)^2 + 5\right]\frac{I_{Y_\parallel}}{I_{Y_\perp}} + \left[45\left(\frac{\alpha}{\beta}\right)^2 + 4\right]}{\left[48\,\frac{\alpha}{\beta} + 8\right]\frac{I_{X_\parallel}}{I_{X_\perp}} + \left[24\,\frac{\alpha}{\beta} + 1\right]\frac{I_{Y_\parallel}}{I_{Y_\perp}} + \left[84\,\frac{\alpha}{\beta} + 8\right]} \right\rangle$$

$$\langle P_4\rangle = \left\langle \frac{\left[-45\left(\frac{\alpha}{\beta}\right)^2 + 84\,\frac{\alpha}{\beta} + 4\right]\frac{I_{X_\parallel}}{I_{X_\perp}} + \left[45\left(\frac{\alpha}{\beta}\right)^2 + 42\,\frac{\alpha}{\beta} + 8\right]\frac{I_{Y_\parallel}}{I_{Y_\perp}} - 1890\left(\frac{\alpha}{\beta}\right)^3 - 180\left(\frac{\alpha}{\beta}\right)^2 - 168\left(\frac{\alpha}{\beta}\right) - 16}{\left[144\,\frac{\alpha}{\beta} + 24\right]\frac{I_{X_\parallel}}{I_{X_\perp}} + \left[72\,\frac{\alpha}{\beta} + 3\right]\frac{I_{Y_\parallel}}{I_{Y_\perp}} + 252\,\frac{\alpha}{\beta} + 24} \right\rangle \quad (7)$$

where

$$\alpha = \frac{1}{3}\,(\alpha_1 + \alpha_2 + \alpha_3)$$

$$\beta = \frac{1}{2}\,\sqrt{(\alpha_1 - \alpha_2)^2 + (\alpha_2 - \alpha_3)^2 + (\alpha_3 - \alpha_1)^2} \quad (8)$$

in which α_i are the principle components of the Raman tensor.[16] The α/β can be directly determined from the depolarization ratio of the unoriented, noncrystalline material where $I_{Y_\parallel} = I_{X_\parallel}$. Then

$$\frac{I_{Y_\perp}\ (\text{unoriented, noncrystalline})}{I_{Y_\parallel}\ (\text{unoriented, noncrystalline})} = \frac{3}{4 + 45\left(\frac{\alpha}{\beta}\right)^2} \quad (9)$$

Wang and Cavanaugh[10] argued that α/β is nearly independent of temperature such that the value obtained in the melt can be used to represent α/β at room temperature. Vasko and Koenig[8] determined the depolarization ratios for all major bands in the Raman spectrum of iPP, and these are shown in Table I.

Equation (7) was used to calculate P_2 and P_4 from the measured intensities for $X_\perp$, $X_\parallel$, $Y_\perp$, and $Y_\parallel$. From eq. (9) it is obvious that there are two

Table I α/β for iPP Raman Bands in Study

Raman Band (cm^{-1})	Depolarization Ratio[a]	α/β Equation (9)	α/β Criteria 10
399	0.080	±0.863	±0.863
454	0.220	±0.463	
809	0.290	±0.375	+0.375
841	0.140	±0.622	±0.622
974	0.810	0	
1152	0.700	0.080	+0.080
1169	0.700	0.080	+0.080
1330	0.770	0	0
1435	0.760	0	0
1457	0.760	0	0

The largest possible depolarization ratio was 0.75, which gave $\alpha/\beta = 0$.

[a] From Vasko and Koenig.[8]

roots for α/β, giving two values of P_2 and P_4. The correct root can be determined by noting that if $\alpha/\beta = 0$, both roots are the same. When $\alpha/\beta \neq 0$, the criteria listed in eq. (10) can be used to select the appropriate value.

$$-0.5 \leq P_2 \leq 1.0$$
$$-3/7 \leq P_4 \leq 1.0 \quad (10)$$

Only solutions compatible with these criteria are acceptable and are listed in the last column of Table I. For the Raman bands at 454 and 974 cm^{-1} neither solution was acceptable, indicating that these values of α/β were not compatible with the data in the present study.

All valid combinations of P_2 and P_4 for all of the bands studied were tested for their correlation with the birefringence. Only P_2 and P_4 of the 1169 cm^{-1} Raman band ($\alpha/\beta = +0.080$) and the P_4 of the 841 cm^{-1} Raman band ($\alpha/\beta = +0.622$) gave good correlations with Δn. Of these, the P_4 of the 841 cm^{-1} band gave the best fit:

$$\Delta n = 0.0756 - 0.218 \cdot P_4 \quad (11)$$

which is shown in Figure 7. The root mean square (RMS) error for this fit was 0.0037. The 841 and 1169 cm^{-1} bands have type A symmetry and approximately 30% of their potential energy distributions consist of the C—C—C backbone stretch. They were measured so that their polarization direction was parallel to the helix axis of iPP.[17]

The only other Raman bands that contain the C—C—C backbone stretch are the bands at 972, 1044, 1365, 1378, 809, and 1152 cm^{-1}. The P_2 and P_4 of the 972 band could not be determined because several samples had calculated P_2 and/or P_4 values that were outside of the possible limits when using the value of α/β provided by Vasko and Koenig.[8] The bands at 1044, 1365, and 1378 cm^{-1} are very weak and thus were not used in this work. The two remaining bands (809 and 1152 cm^{-1}) have type E symmetry and have polarization directions perpendicular to the helix axis. Thus, the birefringence is well correlated to P_2 and/or P_4 of the Raman bands that are polarized parallel to the helical axis of iPP and whose vibration contains a large portion of the backbone C—C—C stretch.

However, the determination of P_4 is cumbersome because spectra have to be recorded in all four experimental geometries. A simpler approach is desirable for routine use, such as in quality control. These above findings suggest that an empirical approach using only the Raman bands associated with the backbone stretch could be used to correlate with the birefringence. However, no satisfactory correlation could be found using only the $Y_\parallel$ spectra, presumably because the band intensities are related to both the orientation and the density. Using the $Y_\parallel$, $X_\parallel$, $Y_\perp$, and $X_\perp$ intensities, the best correlations obtained were

$$\Delta n = 0.1906\left(\frac{I_{Y_\perp}}{I_{Y_\parallel}}\right)_{841} + 0.00259\left(\frac{I_{Y_\parallel}}{I_{Y_\perp}}\right)_{809} - 0.01935 \quad (12)$$

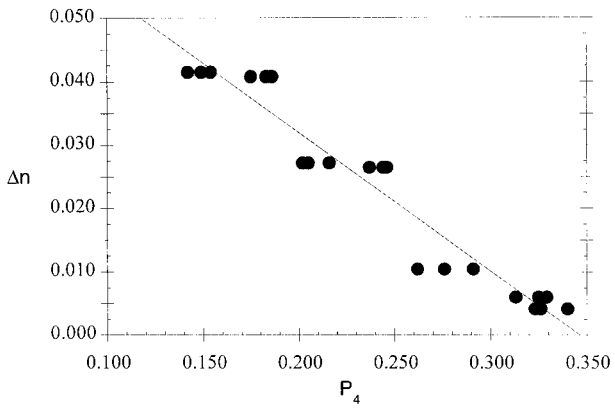

Figure 7 The linear regression of the birefringence with the fourth Legendre polynomial (P_4) of the 841 cm^{-1} Raman band.

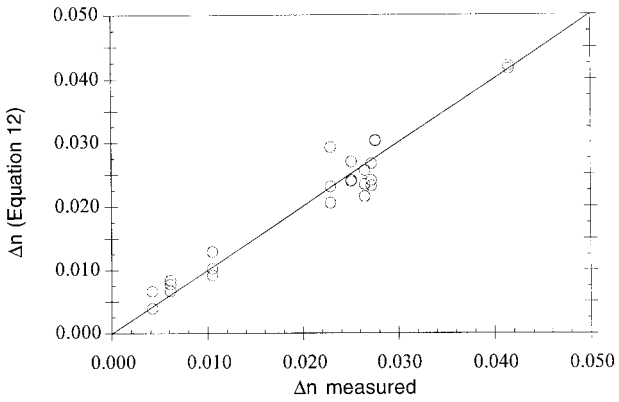

Figure 8 The birefringence calculated according to eq. (12) is plotted against the measured birefringence; (—) a perfect correlation.

where $I_{Y_\parallel}$ and $I_{Y_\perp}$ are the intensities of the vibrational band indicated in the $Y_\parallel$ and $Y_\perp$ experimental geometries, respectively. The RMS error for this fit was 0.0026, which was substantially better than that obtained using P_4. Figure 8 shows the birefringence predicted using eq. (12) compared to the measured values. Because the vibrations of the 809 and the 841 cm^{-1} bands contained the C—C—C backbone stretch, it seemed reasonable that they should occur in this correlation. Furthermore, the Raman tensors for these two bands were predicted to lie nearly perpendicular to each other. It was not surprising that they appeared in eq. (12) with a reciprocal relationship: the 841 cm^{-1} band intensities appeared in the ratio $I_{Y_\perp}/I_{Y_\parallel}$ while the 809 cm^{-1} band intensities appeared in the ratio $I_{Y_\parallel}/Y_{Y_\perp}$. A similar approach can be used for density. The best correlation between the Lorentz density (g/mL) and the Raman spectra found in this study was

$$\rho = 0.9420 - 0.06948\left(\frac{I_{Y_\perp}}{I_{Y_\parallel}}\right)_{841} - 0.000706\left(\frac{I_{Y_\perp}}{I_{Y_\parallel}}\right)_{1330} \quad (13)$$

with a RMS error of 0.001 g/mL, and it is shown in Figure 9. This dependence can be understood by noting that as the birefringence increased the density decreased for these fibers (Fig. 1). The ratio $(I_{Y_\perp}/I_{Y_\parallel})_{841}$ increased as the birefringence increased [as in eq. (12)], and hence this term appeared in the density with a negative sign. There are no reports in the literature indicating that an intensity of the 1330 cm^{-1} band correlates with either the birefringence or the density. We found no correlation between the intensity of this band and the birefringence. However, as shown in Figure 5, there was a large difference in this band between the spectra of these two fibers. Because the change did not correlate with orientation, this difference must have been due to differences in the crystallinity or density.

CONCLUSIONS

The birefringence of iPP fibers can be determined using correlations constructed from Raman band intensities obtained from polarized Raman spectroscopy. It was found that the P_4 of the 841 cm^{-1} Raman band provided a good correlation with the birefringence. The vibration associated with this band involved the backbone C—C—C stretch and was polarized parallel to the iPP helix. The P_2 and P_4 of the other vibrational bands that were polarized parallel to the helix and that included the C—C—C stretch also correlated well with the birefringence. These measurements required the use of four experimental geometries to obtain the required intensities, which was experimentally difficult. A simpler experimental protocol was developed using empirical equations to relate the intensities of the Raman bands with the birefringence and the Lorentz density. These correlations required the use of only two experimental geometries with a common fiber orientation. This greatly reduced the difficulty in making these measurements while simultaneously providing improved accuracy. The RMS error of prediction of the birefringence in the

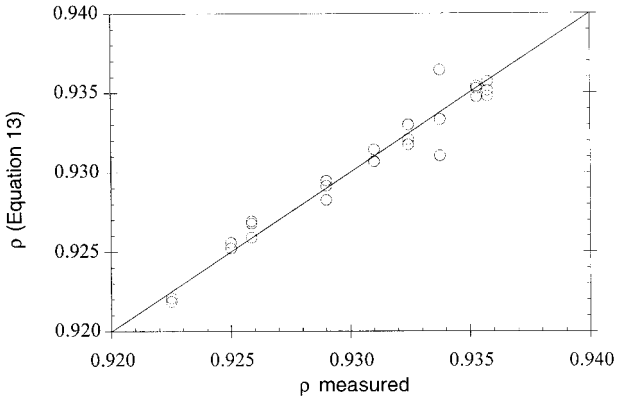

Figure 9 The Lorentz density calculated according to eq. (13) is plotted against the measured Lorentz density; (—) a perfect correlation.

empirical correlation (0.0026) was substantially smaller than that based on the P_4 correlation (0.0037). The RMS error for the Lorentz density correlation was 0.001 g/mL. Thus, the birefringence and Lorentz density of iPP could be determined quantitatively via the correlations developed with Raman microspectroscopy. This provided a new method for determining the morphology of iPP in complex structures, which are not amenable to traditional characterization methods.

The authors would like to thank the Nonwoven Cooperative Research Center for funding this work. In addition, we would like to thank R. Lannigan and P. Desai of FiberVisions for providing the fiber samples.

REFERENCES

1. Natarajan, S.; Michielsen, S. Textile Res J 1999, 69, 903.
2. Natarajan, S.; Michielsen, S. J Appl Polym Sci 1999, 73, 943.
3. Michielsen, S. In 2000 Beltwide Cotton Conferences Proceedings, Cotton and Other Organic Dusts Conference, San Antonio, TX; Wakelyn, P. J., Jacobs, R. R., Rylander, R., Eds.; National Cotton Council of America, Memphis, TN, 2000; Vol. 1, p 192.
4. Schmidt, P.; Hendra, P. J. Spectrochim Acta 1994, 50A, 1999.
5. Purvis, J.; Bower, D. I. J Polym Sci Polym Phys Ed 1976, 14, 1461.
6. Morton, W. E.; Hearle, J. W. S. Physical Properties of Textile Fibers; The Textile Institute: Manchester, U. K., 1993; p 573.
7. Hendra, P. J.; Willis, H. A. Chem Ind (Lond) 1967, 51, 2146.
8. Vasko, P. D.; Koenig, J. L. Macromolecules 1970, 3, 597.
9. Satija, S. K.; Wang, C. H. J Chem Phys 1978, 69, 2739.
10. Wang, C. H.; Cavanaugh, D. B. J Appl Phys 1981, 52, 6003.
11. Arruebarrena de Baez, M.; Hendra, P. J.; Judkins, M. Spectrochimica Acta Part A 1995, 51, 2117.
12. Fraser, G. V.; Hendra, P. J.; Watson, D. S. Spectrochim Acta 1973, 29A, 1525.
13. Operation Manual for the Aus Jena Interphako Interference Microscope; Martin Microscope Company: Easley, SC.
14. DeVries, H. Colloid Polym Sci 1979, 257, 226.
15. Michielsen, S. In Handbook of Raman Spectroscopy; Lewis, I. R., Edwards, H. G. M., Eds.; Marcel Dekker: New York, 2000.
16. Bulkin, B. J. In Analytical Raman Spectroscopy; Brasselli, J. G., Bulkin, B. J., Eds.; Wiley: New York, 1991; p 1.
17. Painter, P. C.; Coleman, M. M.; Koenig, J. L. The Theory of Vibrational Spectroscopy and Its Applications to Polymeric Materials; Wiley: New York, 1982; p 382.